SCANNING ANTENNAS

Electronically scanning antennas are usually arrays of elements, with the elements excited in a progressive phase across the array in a given direction; this scans the beam in that direction. Such an array is called a *phased array.* The array usually produces a narrow (pencil) beam, with modest or low sidelobes. Arrays that produce a shaped beam are usually not scanned. (Related articles are ANTENNA ARRAYS, MULTIBEAM ANTENNAS, and ACTIVE ANTENNAS.) Advantages of phased arrays include the ability to scan and track at rapid rates, the ability to easily and quickly modify beam shape, and the flat physical form of the planar array. Mechanically steered arrays or dishes require a much larger volume. Applications are eclectic, including communication and tracking of nonstationary satellites, earth mapping synthetic aperture radar from aircraft or satellite, airport surveillance radar, ship and aircraft radar and electronic countermeasures, and finally missile defense.

Important array factors for the systems designer are pattern, gain versus angles, element input impedance, and efficiency. In general, each element of an array will have a different input impedance. For a fixed beam array these are called *embedded impedances;* the obsolete and misleading term *active impedance* is deprecated. Not only does a scanning array have different element impedances, but each of them varies with scan angle. These element input impedances are called *scan impedances.* The pattern of array gain versus angles is called *scan element pattern;* this term replaces *active element pattern.* The scan element pattern (SEP) is an extremely useful design factor. The element pattern and mutual coupling effects are subsumed into the scan element pattern; the overall radiated pattern is the product of the scan element pattern, and the pattern of an isotropic array of elements that is scanned to the proper angle. The isotropic array factor incorporates the effects of array size and array lattice, while the *scan element pattern* as mentioned incorporates element pattern, backscreen if used, and mutual coupling. Since the *scan element pattern* is an envelope of array gain versus scan angles, it tells the communication system or radar designer exactly how the array performs with scan, whether blind angles exist, and whether matching at a particular scan angle is advantageous. At a blind angle the array has zero gain. *Scan element pattern* is used for antenna gain in the conventional range equations. Use of infinite array *scan element patterns* allows array performance to be separated into this SEP and edge effects.

Element options for scanning arrays are mostly low gain: waveguide slots, dipoles, patches, flat TEM horns, and open waveguides. This is because element spacing of roughly halfwave is needed to obviate grating lobes. Elements such as the spiral, helix, log-periodic, Yagi-Uda, horn, and backfire are too large for scanning arrays, except for arrays with very small scan range. It is important to note that array elements may be modified for *scan impedance* compensation, as discussed below.

This article presumes some basic knowledge about antennas; the reader may wish to consult these articles: ANTENNA THEORY, ANTENNAS, APERTURE ANTENNAS, RADAR ANTENNAS, and WAVEGUIDE ANTENNAS.

This article comprises four sections: phased array basics, scanning techniques, mutual coupling effects, and finite arrays. A more extensive treatment of all of these subjects is given in the book by Hansen (1).

PHASED ARRAY BASICS

Notation used here is that common in the literature: λ is wavelength, $k = 2\pi/\lambda$, and angular variables are u and v where

$$\begin{aligned} u &= \sin\theta\cos\phi - \sin\theta_0\cos\phi_0 \\ v &= \sin\theta\sin\phi - \sin\theta_0\sin\phi_0 \end{aligned} \tag{1}$$

Here the spherical coordinates are θ, ϕ, and the beam position is θ_0, ϕ_0. It is sufficient to consider a planar array with even numbers of elements, N and M, along the x and y axes. The pattern is then

$$F(u,v) = \sum_{n=1}^{N/2}\sum_{m=1}^{M/2} A_{\text{nm}} \cos\left(n - \tfrac{1}{2}\right)kd_x u \cdot \cos(m - \tfrac{1}{2})kd_y v \tag{2}$$

with the elements spaced d_x and d_y in a rectangular lattice. Equilateral triangular lattices are sometimes used, because they reduce the element density by 17%. The element pattern, which multiplies Eq. (2), has been omitted. For uniform excitation the pattern becomes simply

$$F(u,v) = \frac{\sin\frac{1}{2}Nkd_x u}{N\sin\frac{1}{2}kd_x u} \cdot \frac{\sin\frac{1}{2}Mkd_x yv}{M\sin\frac{1}{2}kd_y v} \tag{3}$$

Use of low sidelobe designs, such as the Taylor $\overline{n}$, or the Taylor one-parameter, requires the A_{nm} coefficient amplitudes to be properly chosen (2). The coefficients contain the interelement scan phase:

$$\exp[jkd(nu + mv)] \tag{4}$$

This is the progressive phase shift needed to scan the beam.

Beamwidth

The half-power points on a uniform array principal plane pattern are found by putting Eq. (3) equal to $\sqrt{0.5}$. This gives, for all but very small arrays, the 3 dB beamwidth θ_3 as

$$\begin{aligned}\theta_3 = &\arcsin(\sin\theta_0 + 0.4429\lambda/Nd)\\ &- \arcsin(\sin\theta_0 - 0.4429\lambda/Nd)\end{aligned} \tag{5}$$

For large N, this reduces to

$$\theta_3 \simeq 0.8858/Nd\cos\theta_0 \tag{6}$$

Cross-plane beamwidth is nearly constant for large N.

Scan Accuracy

Interelement phase shift is necessary to provide beam scan; the devices that produce this phase shift are called *phasers*. Row and column phasing is the simplest, even for circular planar arrays. Thus each phaser is driven by a command to produce a specified x and a specified y-axis phase. The steering bits affect the precision of the beam steering, control bandwidth, and produce phase quantization lobes. Each of these will be discussed.

The smallest steering increment $\Delta\theta$ is related to the smallest phase bit: $\Delta\theta/\theta_3 \simeq 1/2^M$, where θ_3 is the half-power beamwidth. Note that in this case the largest bit is π. Thus four bits gives a steering least count of 0.0625 beamwidth, or 1/16 of a beamwidth. Adding a bit, of course, decreases the steering increment by a factor of two.

Scan Bandwidth

Bandwidth of an array is affected by many factors, including change of element input impedances with frequency, change of array spacing in wavelengths that may allow grating lobes, change in element beamwidth, and so on. When an array is scanned with fixed units of phase shift, provided by phasers, there is also a bandwidth limitation as the position of the main beam will change with frequency. When the array is scanned with true time delay, the beam position is independent of frequency to first order. But with fixed phase shift, the beam movement is easily calculated. Beam angle θ is simply related to scan angle θ_0 by $\sin\theta = (f_0/f)\sin\theta_0$. For example, a beam at 45° moves from 42.2° to 47.9° over a ±5% frequency excursion.

To calculate steering bandwidth assume that the main beam has moved from scan angle θ_0 to the 3 dB points for frequencies above and below nominal. Let subscripts 1 and 2 represent the lower and upper frequencies. Fractional bandwidth is then given by

$$\mathrm{BW} = \frac{f_2 - f_1}{f_0} = \frac{\sin\theta_0(\sin\theta_2 - \sin\theta_1)}{\sin\theta_1\sin\theta_2} \tag{7}$$

For large arrays we have

$$\mathrm{BW} \simeq \frac{\theta_2 - \theta_1}{\sin\theta_0} = \frac{\theta_3}{\sin\theta_0} \tag{8}$$

The bandwidth is then given by

$$\mathrm{BW} \simeq \frac{0.866\lambda}{L\sin\theta_0} \tag{9}$$

for a uniform array. When the beam angle is 30°, the commonly used formula for fractional bandwidth results:

$$\mathrm{BW} \simeq \frac{2\lambda}{L} \tag{10}$$

As a result, long arrays have smaller bandwidth in terms of beam shift at the band edges.

Adding bits of time delay increases this bandwidth; each bit slightly more than doubles the bandwidth as it must, since the number of bits that provide $kL\sin\theta_0$ gives infinite scan bandwidth (1).

Grating Lobes

The array pattern given above allows the inference that a maximum pattern value of unity occurs whenever $(d/\lambda)u = n$. If d/λ and θ_0 are chosen properly, only one main beam will exist in "visible" space, which is for $-90 \le \theta \le 90°$. Large spacings will produce additional main beams called *grating lobes* (GL); this is because the larger spacing allows the wave from each element to add in phase at the GL angle as well as at the main beam angle. The equation for GL is easily determined:

$$\frac{d}{\lambda} = \frac{n}{\sin\theta_0 - \sin\theta_{\mathrm{gl}}} \tag{11}$$

For half-wave spacing, a GL appears at ±90° for a beam scanned to ±90°. A one wavelength, spacing allows GL at ±90° when the main beam is broadside. The onset of GL versus scan angle is shown in Fig. 1. The common rule that half-wave spacing precludes GL is not quite accurate, because part of the GL may be visible for extreme scan angles.

The pattern of a rectangular lattice with scanning in either principal plane behaves exactly like that of a linear array, just described. For other scan angles the situation is less simple. The u–v plane, sometimes called the *direction cosine*

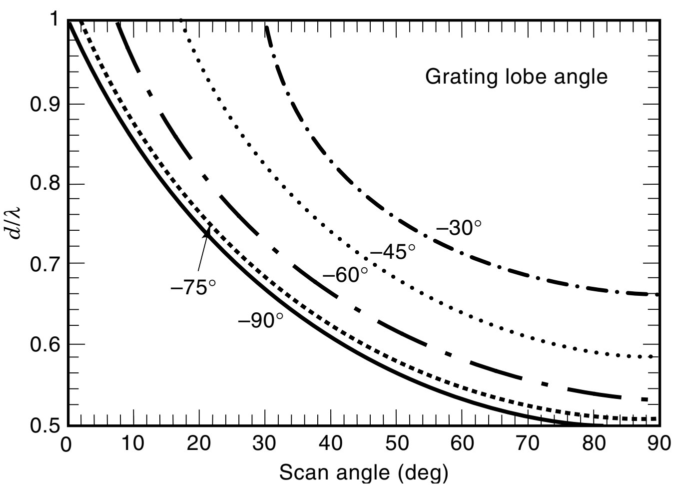

Figure 1. Grating lobe appearance versus element spacing and scan.

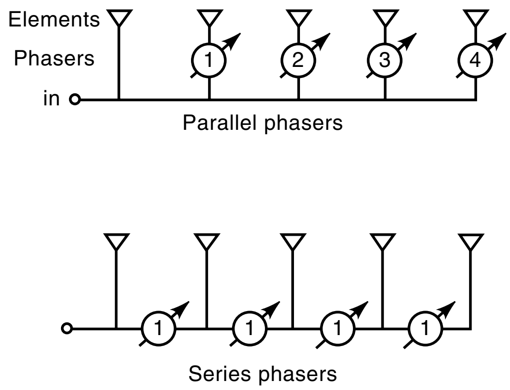

Figure 2. Linear series feeds.

plane, was developed by Von Aulock (3) and is extremely useful for understanding GL behavior. The GL positions can be plotted in the u–v plane; they occur at the points of an inverse lattice, that is, the lattice spacing is λ/d_x and λ/d_y. All real angles, representing visible space, are inside or on the unit circle. The latter represents $\theta = 90°$. Angles outside the unit circle are "imaginary," or in invisible space. When the main beam is scanned, the origin of the u–v plot moves to a new value, and all GL move correspondingly. However, the unit circle remains fixed. For further details on this and on hexagonal lattices, see Hansen (1).

GL can be partially suppressed in one plane of scan for a limited scan range, and over a narrow frequency band, by pseudorandomizing the position of each element. However, the complete two-dimensional pattern, over even a modest bandwidth, will have GL.

SCANNING TECHNIQUES

Phaser Scan

Linear series feeds may be scanned by use of phasers in either the feed line or adjacent to the elements; these are series phasers and parallel phasers. Figure 2 sketches these arrangements. With waveguide slot array sticks there is no room for phaser devices. Many other configurations do allow phasers to be incorporated. An advantage of parallel phasers is that each phaser handles only $1/N$ of the transmitted power, and each element path has the phaser loss. A disadvantage is that the basic interelement phase shift $\phi = kd \sin \theta_0$ must be multiplied by the number of the element. Because almost all phasers are now digitally controlled, this is a minor disadvantage. Modern digital controls are inexpensive. For series phasers the advantage is that all phasers have the same setting equal to ϕ. Disadvantages are that the first phaser must handle almost the entire power and that the phaser losses are in series. In both topologies there are systematic errors due to impedance mismatch. Amplitude taper for sidelobe control is provided through coupling adjustments. A detailed treatment of feed systems is given by Hansen (1).

A word about phasers is appropriate, although a full discussion is outside the scope of this article. Phasers, often called *phase shifters,* are primarily of two basic types: switched line and ferrite. Switched line phasers use semiconductor switches to switch in or out lengths of transmission line, where the latter is usually coax, microstrip, or stripline. Discrete components may be used, but more often the switches, loads, and controls are in integrated circuit packages that are integrated into microstrip or stripline. MMIC configurations are becoming more common, especially above 10 GHz. Of course, these phasers utilize time delay, but because the largest bit is usually 180°, they are classed as phasers. Digital phasers are binary: a 5-bit phaser has phases of 180°, 90°, 45°, 22.5°, and 11.25°. The phaser design must keep the impedances matched as the bits switch, and in extreme applications it must also match the losses. If amplifiers are incorporated to offset losses, the phasers become nonreciprocal.

Ferrite phasers are of two types, and although these are intrinsically analog phasers, current practice has digitized the phase control. They are almost always embodied in waveguide. Toroidal ferrite phasers use one or several ferrite toroids of rectangular shape placed in a waveguide such that the axis of the toroid is along the guide axis. A drive wire threaded through the toroid provides either a positive or negative current pulse. The pulse drives the toroid to saturation, and the toroid is latched at a positive or negative remanent-induction point. The difference between the electrical lengths of the two states provides the phase shift. Typically, several toroids are placed serially with lengths chosen to provide the N bits of phase shift. Advantages and disadvantages are obvious: These phasers are nonreciprocal, and they must be reset after each pulse for radar operation; drive power is used only when switching, so that power and heat dissipation are minimized.

The Faraday rotation ferrite phaser uses a ferrite rod along the axis of the waveguide, with quarter-wave plates at each end to convert linear to circular polarization and vice versa. In practice, the ferrite rod is plated with silver or gold to form a small ferrite waveguide. This ferrite guide is then placed inside the regular guide, with nonplated tapered transition sections on each end to match between the two guides. An external solenoidal coil around the waveguide provides the magnetization that controls the phase shift. Again, typical drive circuits are digitally controlled. These phasers are reciprocal and are often used in high-power applications such as radars. Sophisticated drive compensation circuits have been developed to adjust the drive as the temperature of the ferrite increases; the drive power must be applied at all times. Useful references on phasers include a special issue of MTT transactions on array control devices (4), a chapter on phasers and delayers (5), and a two-volume monograph (6).

Corporate feeds are common in arrays of dipoles, open-end guides, and patches and are named after the structure of organization charts, where the feed divides into two or more paths, then each path divides, and so on. Such feeds are commonly binary, but sometimes the divider tree includes three-way, or even five-way dividers, depending upon the number of array elements. Figure 3 shows a simple binary parallel feed with phasers. As in the case of main-line series feeds, the phase shift needed is progressively larger. Now, however, each path length has only one phaser. For wideband applications, where modulo 2π phase shift is inadequate, time delay units (delayers) can be used, as discussed below. Figure 4 shows a planar patch array, where the microstrip corporate feed lines are visible. Switched-line 3-bit phasers can also be seen.

In a distributed array each element is connected to its own receiver/transmitter module. Such models often contain

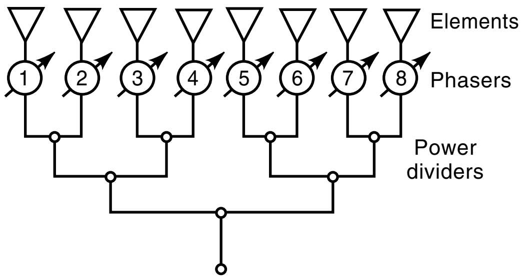

Figure 3. Parallel (corporate) feed. The numbers are phase shift units.

diplexers, circulators, filters, preamps, power amplifiers, phasers, and control components. Sometimes the element is part of the module. Several advantages accrue. Many low-power semiconductor sources may be used instead of a single high-power tube source. Feed network loss, which reduces S/N, is minimized. Graceful degradation allows system operation with slight gain and sidelobe changes as modules fail. MTBF is greatly increased. Against these advantages is the higher cost. The nominal few-hundred-dollar module has been a long-sought goal, but nonrecurring engineering costs are high, especially for MMIC, so that a large number of production units is needed to make the modules cost-effective. Solid-state and tube modules are discussed by Ostroff (7); the current art is reviewed by Cohen (8). Figure 5 shows four generations of x-band modules that feed circular waveguide and TEM horn radiators.

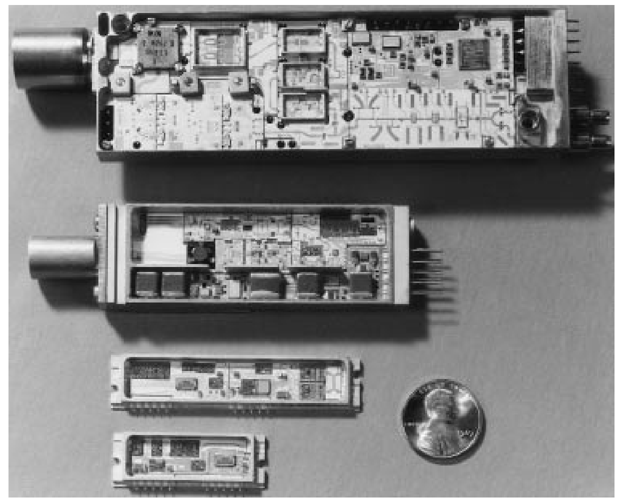

Figure 5. Four generations of modules. (Courtesy of Dr. Chris Hemmi and Texas Instruments.)

Time Delay Scan

Wideband scanning requires time delay, with the maximum amount of delay equal to $(L \sin \theta_0)/c$, where the array length is L, the maximum scan angle is θ_0, and c is light velocity. For example, a 100λ array scanned to 30° needs up to 50λ of delay, or 7 bits of time delay from λ to 64λ. These bits are in addition to the phaser bits below λ; 5 bits of phase gives bits of 11.25° to 180°, making a total of 12 bits to control the array scanning. As mentioned above, many phasers utilize switched lengths of transmission line; time delayers use switched coax or stripline or microstrip. The major problems with microwave delayers are size and loss. Size and weight are important factors, but loss is critical. When a long delay bit is switched in, an amplifier must be controlled to offset the delay loss, so that the array amplitude distribution is not degraded (see article entitled APERTURE ANTENNAS). Long-term and environmental stability are prime concerns with such long delays. An alternate to microwave transmission line delayers is photonic delay, where the delay in a fiber-optic line is used.

Photonic delay lines are used much as microwave delay lines are, with switches to select various delay segments. Of course, optical modulators and detectors are needed; these are discussed in Zmuda and Toughlian (9) and Hansen (1). In the binary delay chain, semiconductor optical switches are used to switch in or out delay segments that are binary multiples of a minimum delay, say 1λ. An n-bit delay chain then provides 1λ, 2λ, 4λ, . . ., $2^{n-1}\lambda$ delays. If phasers are not used for delays below 1λ, the photonic delay chain can include these also. An efficient use of photonic delay is for subarrays only, where each antenna element is connected to a conventional phaser, with largest phase bit of 180°; each subarray is then connected to a photonic delay chain.

Problems encountered in the utilization of photonic delay are connected with uniformity, stability and drift, and IP3. Unfortunately a 1 dB optical nonuniformity produces a 2 dB microwave error. This is because optical intensity produced by a modulator is proportional to microwave current or voltage. IP3 is the third-order intercept point, and it applies to the amplifiers used to offset link loss. An amplifier (extrapolated) gain curve intersects the third-order product gain curve at IP3. The spur-free dynamic range is from the gain curve to the IP3 curve, at the noise floor.

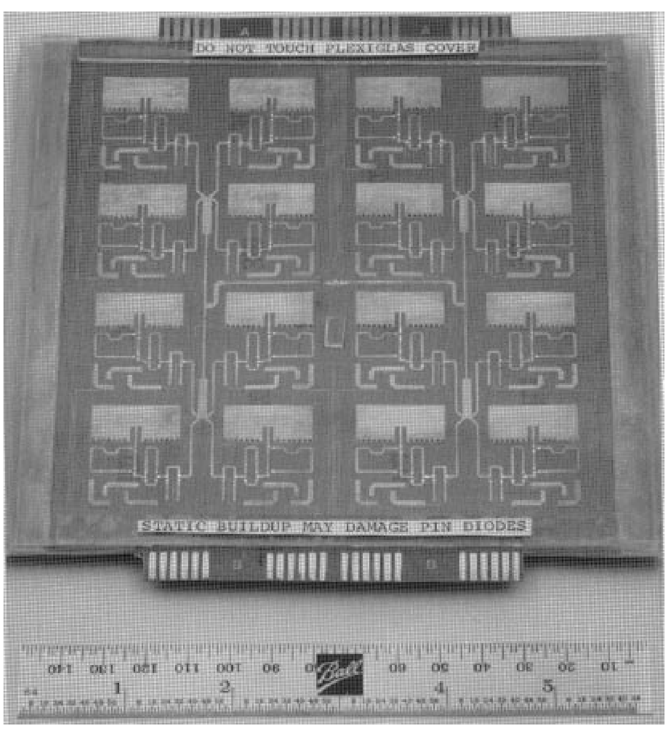

Figure 4. Corporate fed patch array. (Courtesy of Ball Aerospace & Communications.)

An alternative to the use of switched series delays is an N-way "switch" that selects one of N delays. The optical switch is an acousto-optical Bragg cell, in which an applied microwave signal launches a traveling acoustic wave in the acousto-optic crystal. An incident optical beam is modulated by the phonon–phonon interactions and is deflected by an angle proportional to the microwave drive frequency. The optical beam then impinges on one of a cluster of optical fibers, each of which has a binary delay value. Outputs of all the fibers are collected in an optical power combiner, which in turn feeds a photodetector (10).

Delay can be selected by choosing the proper light wavelength, through use of dispersive fibers or through use of frequency selective gratings. The RF-modulated optical beam is sent through a length of highly dispersive fiber; the incremental delay is proportional to the wavelength shift of the laser carrier (11). A representative chromatic dispersion is 50 ps per millimeter of wavelength shift per kilometer of fiber. This dispersion is approximately constant over the laser tuning range. A variable delay can be obtained simply by tuning the laser wavelength, with the delay produced by a length of dispersive fiber. A simple (but expensive) array feed would have a laser oscillator for each array element, with each laser output going through a dispersive fiber and then to a photodetector to the element. Dispersive fiber lengths are of the order of 1 km to 10 km. As mentioned elsewhere, the delay must be stable and accurate to a small part of the smallest phaser bit in the array.

A more elegant architecture utilizes one tunable laser (per plane of scan) with the modulated output fanned out to a cluster of dispersive fibers. These would be designed for delays of τ, 2τ, 4τ, and $(2N-1)\tau$, and each would drive one array element. Tuning the laser would change τ and thus scan the beam. For large arrays the fan-out loss can be appreciable. For two-dimensional scan, two tunable lasers would be used, and the azimuth and elevation delays would be combined at the element photodetectors (12,13).

A grating can be made in a length of fiber by focusing ultraviolet energy onto a periodic sequence of spots along the fiber, thereby producing a grating of spots of different index of refraction. Such a grating will reflect an optical wave at the resonance frequency of the grating. A series of Bragg gratings can be spaced along a fiber, with each reflecting at a different optical wavelength. An optical signal enters the fiber with gratings through an optical circulator; the reflected signal path length (delay) depends upon which grating is selected by the optical frequency. The circulator output then goes to an element, through a photodiode. Thus time delay is controlled by optical wavelength. It should be noted that the photonic delay art is relatively recent, while the microwave feed/phaser art is mature.

Frequency Scan

Advantage can be taken of the beam squint with frequency, by increasing the interelement path length such that a small frequency change scans the main beam. Such arrays are traveling wave arrays, as sketched in Fig. 6. Assume that the radiating elements spaced d apart are connected by a serpentine (snake or sinuous) feed of length s and wave number β. The wavefront is defined by

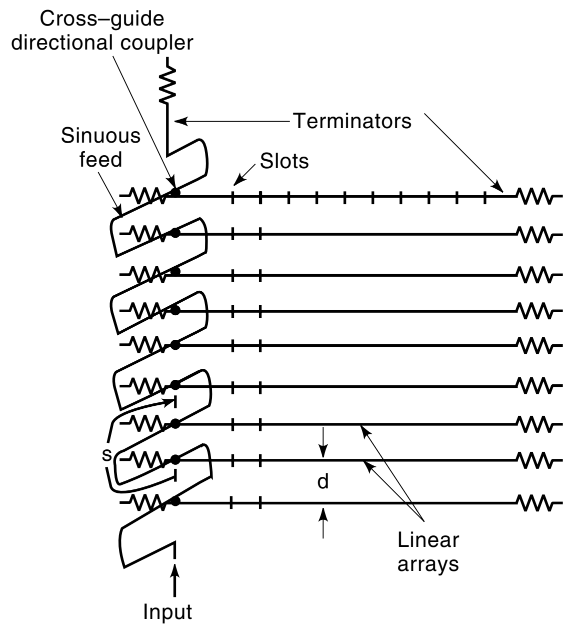

Figure 6. Frequency-scanning sinuous feed feeding an array of traveling-wave linear arrays.

$$kd\sin\theta_m = \beta s - 2\pi m \tag{12}$$

To avoid an endfire beam, $kd \geq \beta s - 2m\pi$. More than one main beam can be avoided by keeping

$$\frac{d}{\lambda} < \frac{1}{1+\sin\theta_m} \tag{13}$$

The phase equation is often written as

$$\sin\theta_m = \frac{s\lambda}{d\lambda_g} - \frac{m\lambda}{d} \tag{14}$$

where λ_g is the serpentine feed wavelength. Clearly larger s/λ, and correspondingly larger m, gives a faster change of beam angle with frequency. If the frequency scan passes through broadside, there will be a significant change in impedance due to the addition of all the element conductances. Element conductances, or couplings, are determined just as for a TW array. If the waveguide bends needed to make a snake are not well-matched over the frequency band, it may be necessary to calculate the input admittance using the techniques developed for resonant arrays. The coupler reflections tend to produce a sidelobe at the conjugate beam direction; the level of this reflection sidelobe depends upon the coupling conductances, and it is higher when the scan is closer to broadside. The signal instantaneous bandwidth must be sufficiently small to avoid beam broadening. Figure 7 shows an early airport surveillance radar antenna.

Quantization Effects

Phaser Quantization Lobes

Most phasers are now digitally controlled, whether the intrinsic phase shift is analog or digital. Such phasers have a least

Figure 7. Airport surveillance antenna. (Courtesy of J. J. Lee and Hughes Aircraft Company.)

phase, corresponding to one bit. An M-bit phaser has phase bits of $2\pi/2^M$, $2\pi/2^{M-1}$, . . ., π. The ideal linear phase curve for electronic scanning is approximated by stair-step phase, producing a sawtooth error curve. Since the array is itself discrete, the position of the elements on the sawtooth are important. There are two well-defined cases. The first case is when the number of elements is less than the number of steps. In this case the phase errors assume a random nature. This can be evaluated by approximating the phase variance by one-third of the peak sawtooth error of $\pi/2^M$. The variance is

$$\sigma^2 = \frac{\pi^2}{3 \cdot 4^M} \tag{15}$$

For uniform excitation of the array the rms sidelobe level is σ^2/N. A modest gain decrease accompanies the increased sidelobes:

$$\frac{G}{G_0} \simeq 1 - \sigma^2 \tag{16}$$

At scan angle θ_0 the main beam is reduced by approximately $\cos^2\theta_0$, so that the rms sidelobe level with respect to the main beam is increased. The second case has two or more elements per phase step, and the discrete (array) case is approximated by a continuous case. This quantization produces a set of lobes called *quantization lobes* (QL), which have predictable amplitudes and positions. An N-element array has an end-to-end phase of $(N-1)\,kd \sin\theta_0$. The number of elements per phase step, with M bits of phase, is J:

$$J = \frac{N}{(N-1)2^M (d/\lambda)\sin\theta_0} \tag{17}$$

This allows the largest scan angle for which $J \geq 2$ to be found. For large arrays N approximately cancels, leaving $\sin\theta_0 \simeq (1/((d/\lambda)\,2^{M+1})$. Larger angles produce pattern errors that are more complex. For J between one and two, there is a transition region between the random sidelobes regime ($J < 1$) discussed and the QL regime.

The QL angle θ_q are governed by the step width W:

$$\frac{W}{\lambda} = \frac{1}{2^M \sin\theta_0} \tag{18}$$

This gives a peak sawtooth error of $\beta = \pi \cdot 2^M$, as mentioned above. The QL amplitudes are given by sinc $(\beta - i\pi)$, where $i = 0$ gives the main beam. The first two QL and the main beam are given by

$$\begin{array}{ll} \text{Main beam:} & \operatorname{sinc}\beta \\ \text{First QL:} & \dfrac{\sin\beta}{\pi \pm \beta} \\ \text{Second QL:} & \dfrac{\sin\beta}{2\pi \pm \beta} \end{array} \tag{19}$$

When $\beta = \pi/2$, the main beam and first QL are equal, clearly a bad case. But this only occurs for one bit phasers, an extreme case. Table 1 gives lobe amplitudes versus number of phaser bits.

Gain decrease is approximate given by the main beam decrease:

$$\frac{G}{G_p} \simeq \operatorname{sinc}^2\beta \tag{20}$$

These data allow the array designer to make an intelligent trade on phaser bits.

For rectangular lattices, the QL appear along the u and along the v axes at the GL angles derived for linear arrays.

There are several schemes for decollimation of phaser QL, of which the best is the phase-added technique (14). In this technique the element phases are calculated to a number of bits that would provide sufficiently low QL if used. Call this number of bits N. The phasers are driven by a smaller number of bits M. A set of random numbers, one for each phaser, with each number N bits long, is generated and stored. The

Table 1. Phaser Quantization Lobe Amplitudes

M	Main Lobe	QL_1	QL_2
1	−3.92	− 3.92	−13.46
2	−0.912	−10.45	−14.89
3	−0.224	−17.13	−19.31
4	−0.056	−23.58	−24.67
5	−0.014	−29.84	−30.38
6	0	−35.99	−36.26

random number table is then truncated to M bits and stored separately. When the set of phaser drive bits is calculated for a given scan direction, the N-bit random numbers are added, one to each phaser drive word. The phaser drive words are then truncated to M bits and the M bit random numbers are then subtracted, one for each phaser drive word. The resulting words are then used to drive the phasers. The result of this is decollimation of the QL, along with a small rise in the average sidelobe envelope. An important advantage is that this method, unlike some others, has zero mean value.

Subarray Quantization Lobes

An array composed of contiguous subarrays, when scanned, has a phase consisting of stair-steps, with one step over each subarray. This, just as in the case of digital phasers, produces quantization lobes, except that a subarray has at least two elements. So the QL are always deterministic here. Call the sawtooth width (subarray width) W and call the peak sawtooth error β, as before. For large arrays the discrete subarray may be replaced by a continuous aperture, but with the sawtooth phase. Consider N equal subarrays, and with uniform excitation. The pattern is found by integrating over a subarray, and then summing over the subarrays.

The integration and summation can both be performed in closed form, with the following result:

$$F(u) = \frac{\sin N\pi W}{N\sin \pi W}\operatorname{sinc}\pi v \tag{21}$$

This is immediately recognized as the pattern of a uniform array of N isotropic elements spaced W wavelengths apart, times the pattern of a uniform line source of length W wavelengths, with main beam at $\theta = v = 0$. For W larger than one wavelength, grating lobes will exist from the first factor. These GL have unit amplitudes and positions for $w = 0, 1, 2, \ldots$. Of these the first is the main beam. These lobes are weighted by the sinc beam. The subarray variable is $\beta = \pi v$, and $v = (W/\lambda)\sin\theta_0$. The QL amplitudes, and that of the main beam, are formed from Eq. (21), using this subarray β. The QL locations are approximately at the GL angles:

$$\sin\theta_{\mathrm{gl}} = \sin\theta_0 \pm \frac{m\lambda}{W}, \qquad m = 1, 2, 3, \ldots \tag{22}$$

For example, $(W/\lambda)\sin\theta_0 = 0.025$ gives QL of roughly -32 dB; a value of 0.05 gives -26 dB; a value of 0.1 gives -20 dB.

These results comprise the reasons why these lobes are called QL rather than GL. Although they occur at the GL angles, their appearance and amplitude is a function of scan angle. While GL appear even for zero scan, phaser and subarray quantization lobes do not exist for zero scan. Their amplitude increases with scan. Further GL tend to have high amplitude, diminished from main beam amplitude only by a slowly varying element pattern. QL, on the other hand, are typically much lower than the main beam, and each additional QL is significantly lower than the previous one.

MUTUAL COUPLING EFFECTS

Scan Element Pattern

A most important and useful parameter for large arrays is *scan impedance* (the obsolete term *active impedance* is confusing and is deprecated); it is the impedance of an element as a function of scan angles, with all elements excited by the proper amplitude and phase. From this the scan reflection coefficient is immediately obtained. Array performance is then obtained by multiplying the isolated element power pattern (normalized to 0 dB maximum) times the isotropic array factor (power) times an impedance mismatch factor. The isolated element pattern is measured with all other elements open-circuited. This is not quite the same as with all other elements absent, except for canonical minimum scattering antennas (1). Here it is assumed that the array is sufficiently large that edge effects are negligible and that scan impedance is that for an infinite array. This simple performance expression allows the contributions of array lattice and element spacing, element type, and mutual coupling to be discerned. Unlike *scan impedance,* which is difficult to measure because all elements must be properly excited, *scan element pattern* (SEP) is measured with one element excited and all other elements terminated in Z_0. It is important to note that *scan element pattern* provides the radar or communications systems designer array gain, at the peak of the scanned beam, versus scan angles. The SEP g_s can be calculated from the *scan impedance* Z_s and the isolated element power pattern g_{iso}:

$$g_{\mathrm{s}}(\theta,\phi) = \frac{4R_{\mathrm{s}}(o,o)g_{\mathrm{iso}}(\theta,\phi)}{|z_{\mathrm{s}}(\theta,\phi)+z_{\mathrm{g}}|^2 g_{\mathrm{iso}}(o,o)} \tag{23}$$

For the general case where the generator reactance is not zero, it is appropriate to use the conjugate reflection coefficient. For the special case where the generator impedance is real the SEP can be written as

$$g_{\mathrm{s}}(\theta,\phi) = \frac{R_{\mathrm{iso}}g_{\mathrm{iso}}(\theta,\phi)}{R_{\mathrm{g}}}|1-\Gamma(\theta,\phi)|^2 \tag{24}$$

An often quoted approximation results for SEP needs to be examined. This purports to show a cos θ variation:

$$g_{\mathrm{s}}(\theta,\phi) \simeq \frac{4\pi A_{\mathrm{elem}}}{\lambda^2}\cos\theta_0[1-|\Gamma(\theta,\phi)|^2] \tag{25}$$

where A_{elem} is the unit cell area of the element. Use of spectral domain results for slots and dipoles, show that this expression is exact, provided that no grating lobes exist, the elements are thin and straight, and no higher modes are engendered by the feed. However, the scan behavior of the mis-match factor must not be overlooked. It can be shown that the SEP behavior is closer to $\cos^{1.5}\theta$, the extra power being contributed by the impedance mismatch. So it is better to use the generally applicable formula for SEP to get accurate and useful results. Extensive scan impedance data for dipole arrays are given by Hansen (1).

Floquet's theorem for arrays states that an infinite regular periodic structure will have the same fields in each cell except for a progressive exponential multiplier. Furthermore, the fields may be described as a set of orthogonal modes. In essence the boundary conditions are matched in the Fourier transform domain, resulting in some cases in an integral equation reducing to an algebraic equation. Each element is contained in a unit cell, with all cells alike and contiguous. The periodic cell approach has proved to be the most powerful and perceptive technique for understanding and for designing

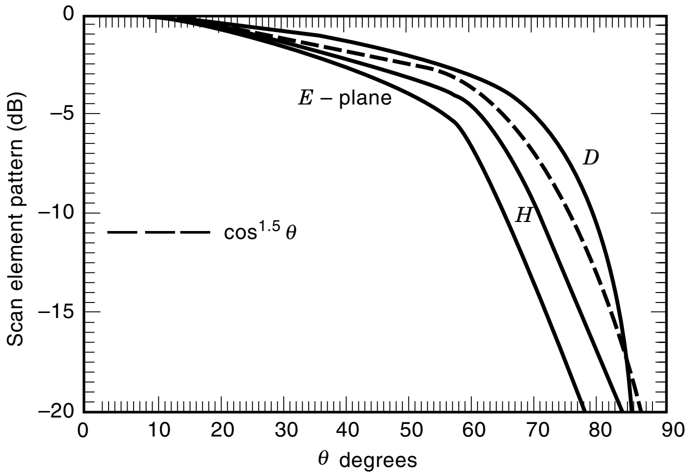

Figure 8. SEP, dipole array. $dx = dy = 0.5\ wv$, $l = 0.5\ wv$.

sophisticated arrays. Because of the Floquet symmetry, the single unit cell contains the complete admittance behavior of each element in the array.

Graphs of scan impedance and SEP give insight into how arrays work as scan angle and lattice spacing are changed. Figure 8 shows SEP for thin half-wave dipoles on a half-wave square lattice. The SEP shows more decrease with scan angle in the *E*-plane, due to the increasingly poor mismatch. A comparison of the SEP with powers of cos θ shows that the best fit is $\cos^{1.5}\theta$; this power pattern lies roughly between the *H*-plane and *E*-plane curves. Note that slot parameters are obtained from those of the dipole by multiplying by a constant. Adding a ground plane raises the broadside scan resistance, but most important it removes the *H*-plane trend to infinity. This is offset by the screen pattern factor, with the result that the SEP for dipoles/screen (Fig. 9) is worse for all planes than that of the dipole array (Fig. 8). Again, the $\cos^{1.5}$ power pattern is a good fit out to about 50° scan; beyond this the SEP falls rapidly due to the screen factor.

Behavior at grating lobe onset is illuminating; the SEP shows a blind angle there for *H*-plane scan. The *E*-plane and

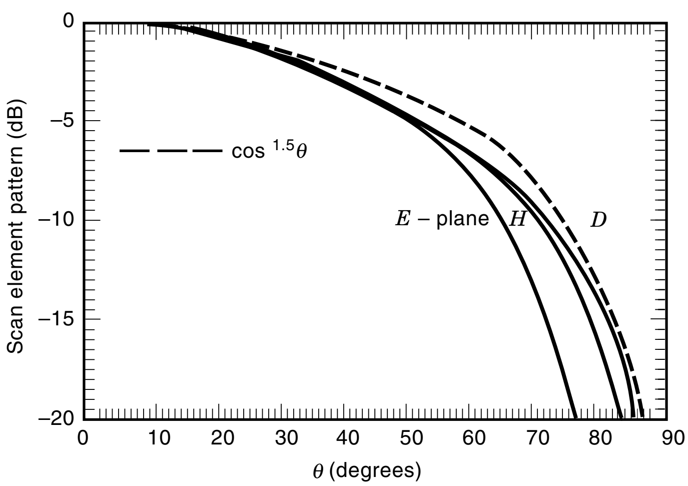

Figure 9. SEP, dipole/screen array. $dx = dy = 0.5\ wv$, $l = 0.5\ wv$, $h = 0.25\ wv$.

diagonal plane scans are only slightly affected. Adding a screen replaces the infinite singularities by a roughly 3 dB dip at grating lobe onset; other planes are not much affected. Clearly, for wideband operation a screen is essential. Behavior for other lattice spacings is similar about the grating lobe onset angle(s). The blind angle occurs because the reflection coefficient there is unity magnitude (1).

Waveguide Simulators

A simple microwave tool that allows the measurement of scan impedance in one scan direction and for one frequency is the waveguide simulator, developed by Brown and Carberry (15) and by Hannan et al. (16). There are some symmetry planes and scan angles that allow perfectly conducting unit cell walls. These walls can then be a metallic waveguide, terminated in a section of the array containing a small number of elements. Another way of visualizing the process utilizes the decomposition of a TE_{01} waveguide mode into two plane waves that reflect off the side walls. The angle of the plane wave with the guide axis corresponds to the θ_0 scan angle. When neither mode index is zero, an additional pair of plane waves reflect off the broad walls (17). For the less often used triangular waveguide simulator, there are three sets of plane waves involved. In a rectangular waveguide simulator the dominant modes allow principal plane scans, while diagonal plane scans require higher modes.

A typical simulator consists of a transition section from standard guide to the simulator guide, the simulator waveguide, and the element port. Across the end of the simulator waveguide is placed a thin metallic sheet with the slot elements appearing as holes. Behind this sheet is a waveguide that encompasses all the complete elements, and that is terminated in a matched load; this is called the *element port.* For elements other than slots or for complex element structures, the element plate is modified accordingly. Careful matching of the transition section is important. The simulator waveguide must be sufficiently long to allow decay of evanescent modes. All diagonal plane simulators contain some fractional elements, because the simulator waveguide is always larger than the array unit cell. Most simulators use rectangular or square waveguide as the modes are simple and the connection to standard guide is easy. Because the waveguide mode constituent plane waves reflect in the *H*-plane, simulation of *H*-plane scan, either in a principal plane or in a diagonal plane, is direct. Conversely, since there is no situation where there are only two plane wave constituents that reflect in the *E*-plane, there are no linearly polarized *E*-plane simulators. Approximate simulation in the *E*-plane will be discussed below.

From the previous discussion it is clear that each simulator provides limited scan impedance data, although frequency variation may provide limited additional data. Thus the choice of the fewest and most economical simulators for a given application is like a chess game, as observed by Wheeler (18).

Figure 10 shows simulators for a square lattice array (16). The *H*-plane tools use the TE_{10} mode, and are principal plane (*C*) or diagonal plane (*IC*). The TM_{11} mode is used in the *E*-plane tools.

Simulation of a broadside beam is not possible; small angles require large simulators. Also *E* polarization produced by a linear element cannot be simulated exactly. The *E*-plane

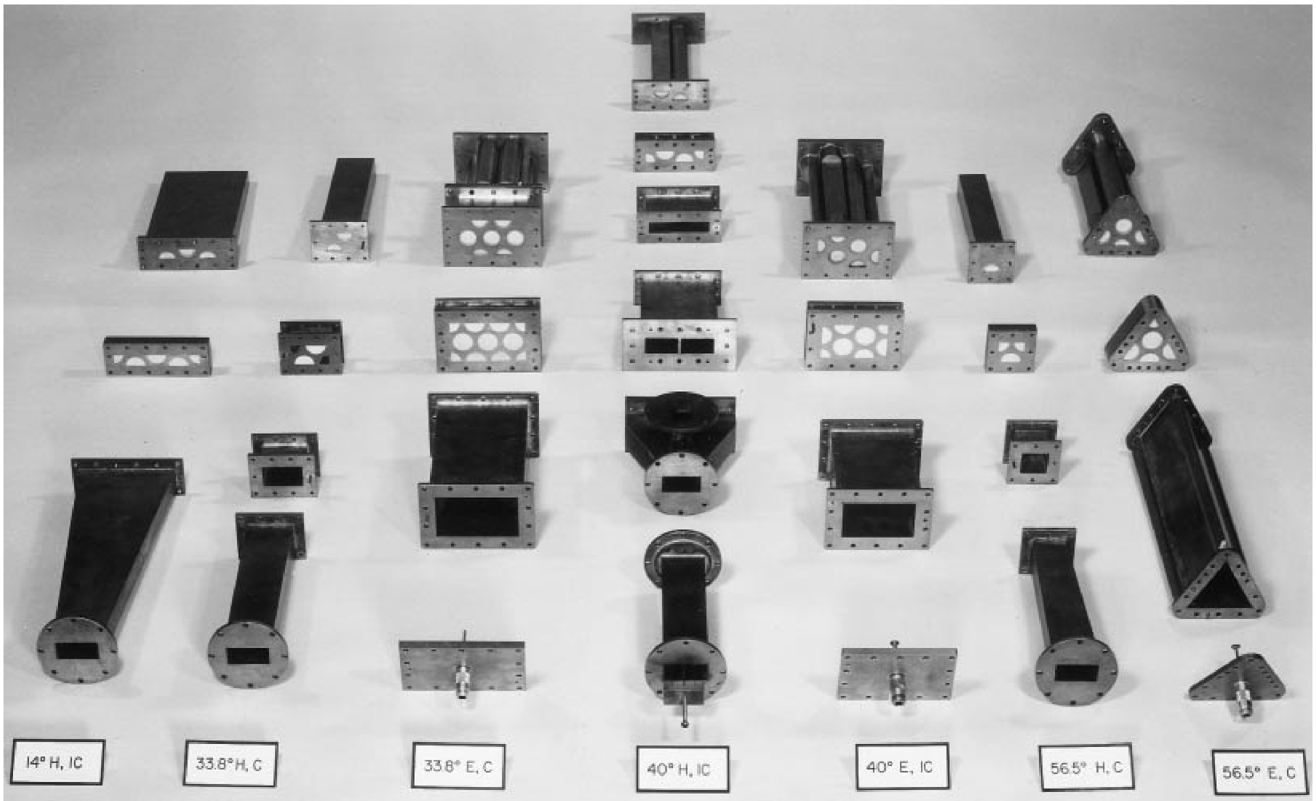

Figure 10. Rectangular lattice waveguide simulators. (Courtesy of Peter Hannan and Hazeltine Corporation.)

simulators previously shown use circularly polarized or cross-linear polarized elements. E-plane simulation in a diagonal plane can utilize a pair of modes, TE and TM, with identical nonzero indices. A detailed review of waveguide simulator design and practice has been given by Wheeler (18). Microstrip patch arrays have also been simulated. Solbach (19) used two H-plane waveguide simulators. Here it was important to carefully reproduce the patch feeds and load resistances.

Scan Compensation

Some arrays radiate no power at a certain angle; this is called a *blind angle.* This phenomenon can, like array performance in general, be viewed from the standpoint of either *scan reflection coefficient* or SEP. The *scan reflection coefficient* may develop a magnitude near or equal to unity, or the SEP may be near or equal to zero. The blind angle occurs when a higher mode cancels the dominant mode in the element. Since the relative phase changes rapidly with scan angle, the two modes produce a resonance, with a resonant phase angle that can be defined on the decrease of $|\Gamma|$ with scan angle. The higher mode can be produced by external or internal structure. Examples of external structure causing a blind angle are a dielectric radome covering each element or row of elements, a dielectric sheet placed on the array face, and a dielectric plug protruding from the mouth of each element. In all cases the scan wave impedance at the array face is modified by the external structure so as to produce a dominant-mode and higher-mode resonance at a particular scan angle; the higher mode exists primarily outside the face. Examples of internal structure that can allow a higher mode that can cause a blind angle are dielectric plugs flush with the array face, dielectric-loaded waveguide elements (as opposed to a short plug), and a brick array of rectangular guide elements. For these various structures the waveguide element supports the next higher mode, which causes the resonance at the blind angle. For the brick array the higher mode is just below cutoff due to the large guide size.

A surface wave can be excited on the dielectric substrate supporting a patch array. The blind angle occurs when the Floquet scan phase velocity matches the surface wave velocity.

Compensation of *scan impedance* changes can be made by any of three different practical methods. These are reduction of coupling, multimode elements, and external wave transformers.

The simplest way to reduce relative coupling uses H-plane baffles between slots or dipoles (20). These baffles are simply metal strips perpendicular to the ground plane and running between the dipoles or slot rows in the H-plane.

The ideal element power pattern of cos θ implies that both TE and TM modes are needed in the array unit cell. The additional modes can be produced by modifying the radiating element in any of several ways. Probably the most effective way of producing the optimum mix of modes uses open-end waveguide radiators, rectangular or circular, with the waveguide internal environment suitably modified. A dielectric plug can be placed at the rectangular waveguide width, and height steps (in different planes) are also used. The mix of modes that is needed depends upon the waveguide and lattice dimensions. With a dielectric plug in the waveguide the TE_{20}

mode will likely be propagating; all other higher modes will be evanescent. The plug should be a half-wave long (in loaded guide wavelengths) at center frequency to properly locate the scan admittance on the Smith chart. Then the guide dimensions are adjusted to give a high susceptance for the TE_{20} mode looking into the matching network. Steps in guide height can then be used for center angle impedance matching; additional dielectric plugs can also be used for matching.

Another scheme combines the TE and TM radiators: a longitudinal shunt slot with parasitic monopoles with L-shaped extensions developed by Clavin et al. (21). The monopoles reduce the E-plane beamwidth and add an electric-type mode to complement the slot magnetic-type mode. Patterns in E- and H-plane can be made equal. Mutual coupling between elements is reduced, and the array wide-angle sidelobes and backlobe are significantly reduced.

A different use of a dielectric sheet involves placing a high dielectric constant thin sheet near the array face. This technique, called *wide-angle impedance matching* (WAIM), uses the susceptances of the sheet to equalize part of the aperture susceptance variation with scan. This is possible because the sheet susceptance varies differently in the E-plane and H-plane. An optimum match is obtained by adjusting the sheet thickness t (for a given ϵ_r) and the sheet spacing from the array face to minimize SEP variations over the scan volume.

The array SEP may be altered through use of a spatial filter or transformer placed in front of the array face, but sufficiently far away that the filter does not directly affect element impedances. The transfer function of the spatial filter is designed to compensate the SEP variations; polarization effects may also be improved. With dielectric sheets the transmission coefficient varies differently with angle in E- and H-planes, so that in principle one or more sheets could improve the SEP (22).

FINITE ARRAYS

Edge Effects

Although the infinite array techniques previously discussed are excellent for system trades and preliminary design, final design requires a finite array simulation. For thin half-wave dipoles or narrow slots, for example, sizable planar arrays may be solved using direct impedance methods; moment methods are not necessary. When the element current distribution is complicated, the number of moment method expansion functions needed for good convergence will restrict this method to small arrays. A discussion of other methods as well as these is given by Hansen (1).

Using the impedance matrix approach, Diamond (23) computed scan impedance and SEP of several small arrays of dipoles. Small arrays exhibit behavior that oscillates around that of a large array. In general, as might be expected, larger arrays have more oscillations, but of smaller amplitude.

Gibbsian Model

A computer simulation of dipole and of dipole/screen arrays showed that the oscillations in scan impedance across the finite array occur even at broadside (no scan) and that they closely resemble the Gibbs phenomenon. This is the oscillations in a square wave represented by a band-limited function. They are largest at the edges (of the square wave and of the array) and diminish away from the edge. The Gibbs amplitudes are given by the Sine Integral, with extrema occurring for arguments of $n\pi$ (24). The period of the oscillations in *scan impedance* increases with scan angle, as $1/(1 - \sin\theta_0)$, both in the simulated results and in the model. This mode was derived from the Fourier transform of a single pulse with a linear phase, and it also utilizes Sine Integrals. Simple finite array models using the Gibbsian form have been constructed, with good comparisons with simulated results (25).

BIBLIOGRAPHY

1. R. C. Hansen, *Phased Array Antennas,* New York: Wiley-Interscience, 1998.
2. R. C. Hansen, Array pattern control and synthesis, *Proc. IEEE,* **80**: 141–151, 1992.
3. W. H. Von Aulock, Properties of phased arrays, *Proc. IRE,* **48** (10): 1715–1727, 1960.
4. L. R. Whicker, (ed.), Special issue on microwave control devices for array antenna systems, *IEEE Trans. Microw. Theory Tech.,* **MTT-22**: 589–708, 1974.
5. W. J. Ince and D. H. Temme, Phasers and time delay elements, In L. Young (ed.), *Advances in Microwaves,* Vol. 4, New York: Academic Press, 1969, pp. 1–189.
6. S. K. Koul and B. Bhat, *Microwave and Millimeter Wave Phase Shifters,* Vols. I and II, New York: Artech House, 1991.
7. E. D. Ostroff, *Solid-State Radar Transmitters,* New York: Artech House, 1985.
8. E. D. Cohen, Trends in the development of MMICs and packages for active electronically scanned arrays (AESAs), In *Proc. IEEE Symp. Phased Array Syst. Technol.,* Boston, MA, 1996, pp. 1–4.
9. H. Zmuda and E. N. Toughlian (eds.), *Photonic Aspects of Modern Radar,* New York: Artech House, 1994.
10. W. D. Jemison and P. R. Herczfeld, Acoustooptically controlled true time delays, *IEEE Microw. Guided Wave Lett.,* **3** (3): 72–74, 1993.
11. R. A. Soref, Optical dispersion technique for time-delay beam steering, *Appl. Opt.,* **31**: 7895–7897, 1992.
12. S. T. Johns et al., Variable time delay of microwave signals using high dispersion fiber, *Elect. Lett.,* **28**: 555–556, 1993.
13. M. Y. Frankel, P. J. Matthew, and R. D. Esman, Two-dimensional fiber-optic control of a true time-steered array transmitter, *IEEE Trans. Microw. Theory Tech.,* **MTT-44**: 2969–2702, 1996.
14. M. S. Smith and Y. C. Guo, A comparison of methods for randomizing phase quantization errors in phased arrays, *IEEE Trans. Antennas Propag.,* **AP-31**: 821–827, 1983.
15. C. R. Brown and T. F. Carberry, A technique to simulate the self and mutual impedance of an array, *IEEE Trans. Antennas Propag.,* **AP-11**: 377–378, 1963.
16. P. W. Hannan, P. J. Meier, and M. A. Balfour, Simulation of phased array antenna impedance in waveguide, *IEEE Trans. Antennas Propag.,* **AP-11**: 715–716, 1963.
17. R. E. Collin, *Foundations for Microwave Engineering,* New York: McGraw-Hill, 1966.
18. H. A. Wheeler, A survey of the simulator technique for designing a radiating element, In A. Oliner and G. H. Knittel (eds.), *Phased Array Antennas, Proc. 1970 Phased Array Antenna Symp.,* New York: Artech House, 1972, pp. 132–148.
19. K. Solbach, Phased array simulation using circular patch radiators, *IEEE Trans. Antennas Propag.,* **AP-34**: 1053–1058, 1986.
20. S. Edelberg and A. A. Oliner, Mutual coupling effects in infinite planar arrays. Part I, Slot arrays; and Part II, Compensation effects, *IRE Trans.,* **AP-8**: 286–297, 360–367, 1960.

21. A. Clavin, D. A. Huebner, and F. J. Kilburg, An improved element for use in array antennas, *IEEE Trans. Antennas Propag.,* **AP-22**: 521–526, 1974.
22. B. A. Munk, T. W. Kornbau, and R. D. Fulton, Scan independent phased arrays, *Radio Sci.,* **14**: 979–990, 1979.
23. B. L. Diamond, Small arrays—Their analysis and their use for the design of array elements, In A. A. Oliner and G. H. Knittel (eds.), *Phased Array Antennas, Proc. 1970 Symp.,* New York: Artech, 127–131, 1972.
24. H. S. Carslaw, *An Introduction to the Theory of Fourier's Series and Integrals,* New York: Macmillan, 1930.
25. R. C. Hansen and D. Gammon, Standing waves in scan impedance of finite scanned arrays, *Microw. Opt. Technol. Lett.,* **8**: 175–179, 1995.

R. C. Hansen
R. C. Hansen, Inc.

SCANNING ELECTRON MICROSCOPES. See Electron microscopes.

SCATTERING. See Electromagnetic wave scattering.

SCATTERING AND PROPAGATION IN REMOTE SENSING. See Microwave propagation and scattering for remote sensing.

SCATTERING AND PROPAGATION, MICROWAVE. See Microwave propagation and scattering for remote sensing.

SCATTERING IN REMOTE SENSING. See Microwave remote sensing theory.

SCATTERING PARAMETERS. See Attenuation measurement.

SCATTERING, RADAR. See Radar remote sensing of irregular stratified media.